is replaced with a set of conical frustrums. This, together with taking γ constant over each frustrum, allows analytical integration over s_i. Formation of the radial and axial velocities from the stream function, application of the no-normal flow boundary condition at some intermediate point of each frustrum and numerical integration over θ provides a set of simultaneous algebraic equations in the sheet strength. (Note that assuming the γ to be sectionally constant does not provide the free constant usually found in vortex sheet applications. Consequently, there is no opportunity to impose a Kutta condition or some facsimile.) Discrete application of the boundary condition provides for some flow through the sheet, thereby duplicating a porous material.

Once the γ distribution is obtained, velocities anywhere in the field except on the sheet itself may be found from the appropriate ψ derivatives. The surface values would come from the ψ derivatives $\pm\gamma/2$.

3. Application

An indication of the porosity of the mathematical "fabric" may be obtained from application to a solid hemispherical parachute. The calculated mass flow per unit time and area between two points near the portion of the canopy oriented at a 45° angle to the freestream is very nearly the same function of differential pressure for $\Delta p < 100$ psf as is a specimen of MIL-C-7020 TYPE III (Ref. 2). The effective porosity for the entire canopy, defined as the ratio of the average velocity through the cloth to the freestream velocity is 0.042. Results are not significantly different using 24 frustrums than they are for only 12.

Measured[3] and calculated internal surface pressures are shown in Fig. 1 for O'Hara models[4] 3, 5 and 7. There was no agreement between external surface pressure distributions due to flow separation. Mouth plane axial velocities are given for the same geometries in Fig. 2, with the experimental values being obtained through pressure rake surveys.[4] The large variations in computed values toward the skirts are due to the proximity to the edge of the vortex sheet. Vent plane axial velocities[4] agreed well qualitatively, increasing from the centerline values to ones roughly one-third greater at the vent boundary, but the calculated magnitudes were greater by factors of 3 to 4. The measured velocities were somewhat suspect, however, as in no case did they satisfy the conservation of mass. Substitution of the calculated vent plane values would bring measured vent and fabric mass outflows close to the measured inflows.

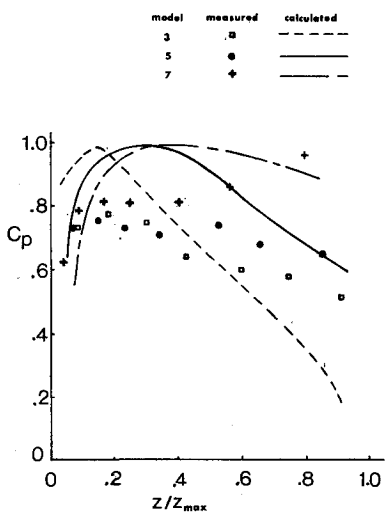

Fig. 1 Internal surface pressure distributions on O'Hara models 3, 5, and 7.

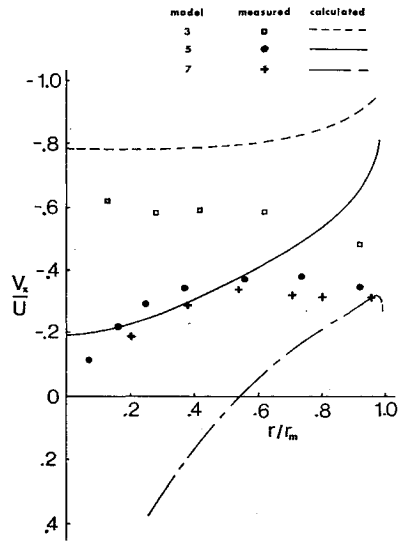

Fig. 2 Mouth plane axial velocities for O'Hara models 3, 5, and 7.

4. Concluding Remarks

These theoretical predictions of internal flow properties are only fair numerically, but they represent general behavior reasonably well. There may be applications where results of this type are more desirable or more available than average or empirically derived quantities.

Although results may be improved by assuming a variable sheet strength distribution, no essential gains in applicability could be expected due to the failure to consider viscosity. Significant advances might be made by adapting the technique to the opening problem. Even in highly viscous fluids, impulsive motions produce flowfields which closely resemble potential flows. The relatively short times involved in the opening problem suggest that an inviscid approximation may be a very realistic one.

References

[1] Milne-Thomson, L. M., *Theoretical Hydrodynamics*, 4th ed., Macmillan, New York, 1966, pp. 552–3.

[2] "Performance and Design Criteria for Deployable Aerodynamic Decelerators," *United States Air Force Parachute Handbook*, TR ASD-TR-61-579, Dec. 1963, Aeronautical Systems Div., Air Force Systems Command.

[3] Heinrich, H. G. et al., "Theoretical Analysis of the Dynamics of the Opening Parachute," Progress Rept. 18, Sept. 1961, Univ. of Minnesota, Minneapolis, Minn. pp. 74–75.

[4] Lockman, W. K., "Analysis of an Inflating Subsonic Reefed Parachute with Experimental Mass Flow Study," Master's thesis, Univ. of Minnesota, Nov. 1963, pp. 19, 119–141, 38.

Study of Rotating Airfoil

HAJI M. JAMEEL*
University of California, Davis, Calif.

Introduction

THE performance of a rotating airfoil depends upon the effects produced due to rotation. Experiments conducted by H. Himmelskamp[1] show the large rotational effects exist near the hub. Himmelskamp assumed these effects to be

Received November 3, 1971.
Index category: Rotary Wing and Aerodynamics.
* Graduate Student, Department of Mechanical Engineering.

due to the centrifugal and Coriolis forces acting in the boundary layer. Recently, Dwyer and McCroskey[2] showed analytically that rotationally induced pressure-gradients, Coriolis forces and cross-flow derivatives are more important than the centrifugal forces.

In the present experimental program, the previous analysis by H. Himmelskamp and by Dwyer and McCroskey has been investigated. Various lengths of a NACA 0012, 2-in. chord-length blade were tested for the lift coefficient. A very sensitive mechanical balance was used to measure the lift. Two-dimensional tests were also conducted in a closed-section wind tunnel using a 20-in.-long blade.

Test Facilities and Conditions

A special apparatus designed for the rotating airfoil studies was used in the test. Reference 3 gives a detailed description of the apparatus. To measure the lift a very sensitive balance with a sensitivity of $\pm 0.1\%$ was used.

During the study, the following conditions were fulfilled: 1) The flow was steady. 2) The fluid followed the perfect gas laws. 3) The viscosity of the fluid was constant. 4) The flow was incompressible. 5) The flow was three-dimensional (two-dimensional for wind-tunnel testing of a stationary blade.) 6) The airfoil was considered to be symmetric. 7) Geometric angle of attack has been taken as the angle between the chord-line and horizontal plane. 8) The velocity of the airstream was assumed to be the velocity of rotating airfoil. In reality, the velocity will be the vector sum of the blade velocity and axial velocity of the airstream.

Various experimental trials were conducted for three different lengths (4-in., 6-in., and 8-in.) of blade at an angular velocity of 600 rpm. The average lift was measured at various angles of attack (geometric). It was found that the accuracy of balance decreased as the length of blade increased, due to the excess vibration. However, in the range of experiments, the lift data were within $\pm 5\%$ of the balance readings. The lift coefficients for the various blades are plotted against the geometrical angle of attack in Fig. 1.

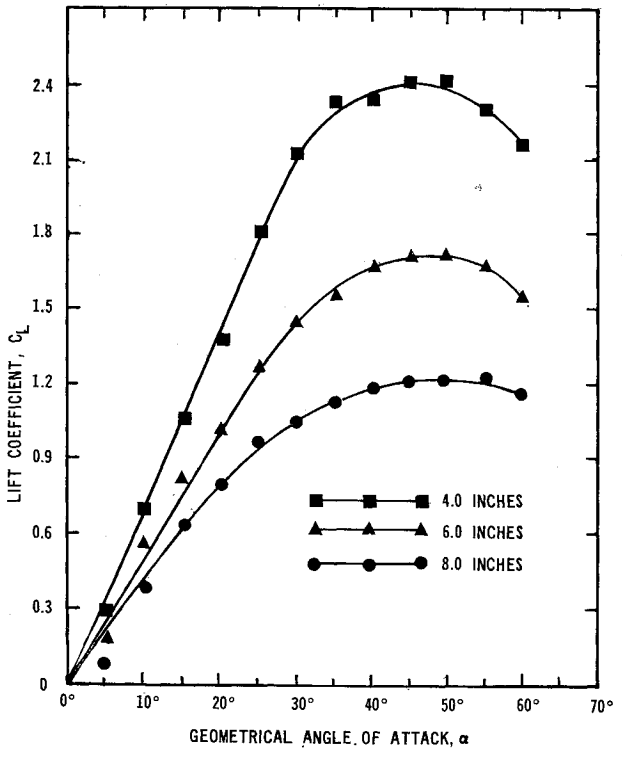

Fig. 1 Lift coefficient C_L for various lengths of rotating NACA 0012 airfoil at various angles of attack (geometric).

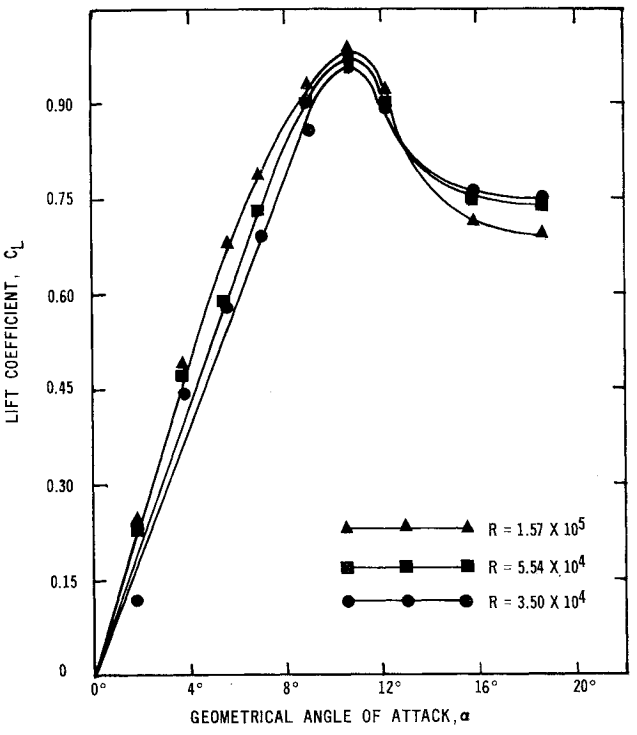

Fig. 2 Lift coefficient C_L at various Reynold's number for two dimensional flow over 20 in. NACA 0012 airfoil in wind tunnel.

A two-dimensional analysis was carried out in a closed-section wind-tunnel at Reynolds number of 3.54×10^4, 5.54×10^4, and 1.57×10^5. A 20-in.-long blade was used for the study. The results thus obtained are shown in Fig. 2.

Test Results and Discussion

Knowing the average values of lift for each blade at different angles of attack (geometric), the lift coefficient is calculated using blade element theory as

$$C_L = L \Big/ \left(n \int_{r_1}^{r_2} 1/2 \, \rho w^2 r^2 dr \right)$$

where n = number of blades (2 for the present case), r = radial distance, $(r_2 - r_1)$ = length of the blade, w = angular velocity (600 rpm), L = lift, and C_L = lift coefficient.

The values of lift coefficients thus obtained are plotted against geometric angle of attack. The effective angle of attack will be less than the geometrical due to the induced axial velocity of the airstream. The lift coefficient obtained is the average over the whole blade.

From the results it can be seen that due to rotation, the separation is being delayed and the maximum lift coefficient is obtained between the goemetric angles of attack of 45° and 50°. The lift coefficients for the smaller blades are more than that for the larger blades. The reason is that the stall occurs earlier at the tip of the blade than near the hub. As a result, the smaller blades stalled later than the large ones. The reason for the increase of lift coefficients for the large blade even after the stall is that the outer portion of the blade has been stalled already, but the inner portion has not. The overall effect will be the slight increase of the lift coefficient.

The two-dimensional data shows that the stall occurs at an angle of attack of 11.5°, whereas the data published by NACA shows that the stall occurs at 12°. This difference is due to the tip effect. The length of the blade was not long enough to cover the whole section of the wind tunnel.

Comparison of the rotating airfoil data with two-dimensional analysis shows that near the stall the lift coefficients for

the rotating airfoils are much higher than that for stationary airfoils in two-dimensional flow. The effect can be traced out to be due to the separation being delayed at larger angle of incidence. The displacement of separation is explained by Dwyer and McCroskey to be due to the appearance of a favorable pressure-gradient, cross-flow derivative, Coriolis forces and centrifugal forces. The Coriolis forces and apparent pressure-gradient are induced by the potential cross-flow. The maximum benefits with regard to separation are due to favorable pressure-gradient, and it will be more when close to the axis of rotation. The detailed explanation is given in Ref. 2.

The slope of the lift curve for two-dimensional flow is larger than the rotating case. Therefore, at smaller angles of attack the stationary blade in two-dimensional flow gives higher lift-coefficient than the rotating one, and is better in performance at those angles. However, at large angles of attack, the rotating airfoil has a better lift-coefficient.

Conclusions

From the results of the investigation the following conclusions can be drawn: 1) The over-all lift coefficient decreases with the increase of blade length. 2) The slope of lift curve for two-dimensional case is larger than the rotating. Lift coefficients at large angles of attack are greater for the rotating case. The rotating blade stalled at higher angle of attack than a stationary blade. 3) The present study confirms the experimental results obtained by Himmelskamp and theoretical results by Dwyer and McCroskey. Hopefully the present study will help pave the way for an extended study of rotating airfoils.

References

[1] Himmelskamp, H., "Profiluntersuchungen an einem umlaufenden Propeller," Diss. Göttingen 1945, Reports of the Max-Planck-Institut für Strömungsforschung, Göttingen, No. 2, 1950.

[2] Dwyer, H. A. and McCroskey, W. J., "Cross-flow and Unsteady Boundary Layer Effects on Rotating Airfoils," *AIAA Journal*, Vol. 9, No. 8, Aug. 1971, pp. 1498–1505.

[3] Jameel, H. M., "The Study of Rotating Airfoils," M. S. thesis, May 1971, Univ. of California, Davis, Calif.

[4] Schlichting, H., *Boundary-Layer Theory*, 6th ed., McGraw-Hill, New York, 1968, pp. 649–653.

[5] Durand, W. F., *Aerodynamic Theory*, Vol. IV, Dover, New York, 1963, pp. 169–293.

Airplane Yaw Perturbations due to Vertical and Side Gusts

ROBERT R. RANKINE JR.*
Air Force Institute of Technology, Wright-Patterson Air Force Base, Ohio
AND
CORNELIUS T. LEONDES†
University of California, Los Angeles, Calif.

AN apparently well-accepted fact pertaining to the analysis of aircraft flight in continuous random turbulence is that the main disturbance to lateral tracking is due to side gusts, and further, that the main contribution of the side gust is accounted for by the sideslip it induces. Consequently, the "beta gust" often has been the sole disturbance input considered in recent airplane turbulence performance studies.[1] Actually, a side gust distribution induces a rigid-body response of the airframe not only by producing an effective sideslip at its center of gravity, but also by producing an effective yaw angular velocity through the linear gradient of the side gust along the aircraft longitudinal axis.[2] Both of these effects must be considered simultaneously if the resultant airframe perturbation in a continuous random side gust is to be realistically determined. As will be shown, the yaw-rate effect of the gust produces considerable low-frequency attenuation of the airframe side-gust response which would be neglected by considering the sideslip effect alone.

The incremental disturbances of sideslip and yaw-rate produced by the continuous random side gust may be mathematically represented by low-pass-filtered white noise as shown in Fig. 1 where n is a white noise signal of unity power spectrum density and the filter dynamics are[2]

$$T_{v_g}(s) = \sigma_v\left(\frac{L_v}{\pi U_0}\right)^{1/2}\frac{1+[(3)^{\frac{1}{2}}L_v/U_0]s}{(1+L_v/U_0 s)^2} \tag{1}$$

$$R(s) = \frac{s}{1+(3b/\pi U_0)s} \tag{2}$$

In these equations U_0 = equilibrium aircraft airspeed, fps; b = wing span, ft; $L_v = \{145\ h^{1/3}$ below $h = 1750$ ft, 1750 above $h = 1750$ ft$\}$, ft, h = altitude, ft; $\sigma_v^2 = L_v\sigma_w^2/L_w$, $(\text{fps})^2$ $L_w = \{h$ below 1750 ft, 1750 above 1750 ft$\}$, ft, and σ_w is the vertical gust intensity, fps.

For an airplane with a 38.4 ft span flying 500 ft above ground level at 520 knots Eqs. (1) and (2) become

$$T_{v_g}(s) = \frac{0.6461\sigma_v(1+2.272s)}{(1+1.312s)^2} \tag{3}$$

$$R(s) = \frac{s}{1+.04179s} \doteq s \tag{4}$$

where the side gust intensity is scaled such that $\sigma_v = 1.517\sigma_w$. The incremental gust disturbances of sideslip and yaw rate enter only the aerodynamic terms of the lateral-directional equations of motion of the aircraft.[2] For example, for a typical tactical fighter at the flight condition considered above the equations in stability axes are:

$$\begin{bmatrix} s+1.313 & -.3614 & 10.59 \\ .0119 & s+.5261 & -10.89 \\ -.0003s-.0345 & .998s & s^2+.2257s \end{bmatrix}\cdot\begin{bmatrix} p \\ r \\ \beta \end{bmatrix} = \begin{bmatrix} -1.313 & .3614 & -10.59 \\ -.0119 & -.5261 & 10.89 \\ .0003s & -.998s & -.2257s \end{bmatrix}\cdot\begin{bmatrix} p_g \\ r_g \\ \beta_g \end{bmatrix} = \begin{bmatrix} -1.313 & (-.3614s+10.59)/877.6 \\ -.0119 & (.5261s-10.89)/877.6 \\ .0003s & (.998s^2+.2257s)/877.6 \end{bmatrix}\cdot\begin{bmatrix} p_g \\ v_g \end{bmatrix} \tag{5}$$

where $v_g = T_{v_g}n$, and the effective roll angular velocity (p_g) due to the spanwise gradient of the continuous random vertical gust has also been included. Again, as with the side gust, the incremental roll-rate disturbance produced by the continuous random vertical gust is mathematically represented by a

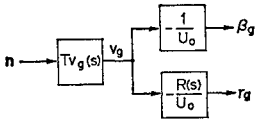

Fig. 1 Mathematical model for the generation of continuous random side gusts and their propagation into equivalent aerodynamic effects.

Received November 15, 1971.
Index categories: Aircraft Handling, Stability, and Control; Aircraft Gust Loading and Wind Shear.

* Major, USAF, and Assistant Professor of Electrical Engineering.
† Professor of Engineering and Applied Science. Member AIAA.